Chemical Science

ROYAL SOCIETY OF CHEMISTRY

EDGE ARTICLE

View Article Online
View Journal | View Issue

Cite this: *Chem. Sci.*, 2025, **16**, 20300

All publication charges for this article have been paid for by the Royal Society of Chemistry

A simple epoxide modification strategy to construct amino-functional poly(2-oxazoline) mRNA delivery vectors

Kuncheng Lv,[ab] Yibo Qi,[ab] Hanqin Zhao,[ab] Yuyan Zhang,[ab] Ziyue An,[ab] Sheng Ma[a] and Wantong Song *[abc]

Messenger RNA (mRNA) delivery vectors are pivotal in the realm of vaccines and gene therapy. While polymer-based delivery vectors have garnered growing interest owing to their tunable structures and favorable biocompatibility, achieving high delivery efficiency remains a critical challenge. Poly(2-oxazoline) (POx) emerges as a promising candidate in biomedicine, yet its exploration in mRNA delivery is nascent. Herein, we engineered poly[2-(5-aminopentyl)-2-oxazoline]-based (PAmOx) polymers as efficient mRNA delivery vectors through a straightforward one-step ring-opening reaction between the amino group on the PAmOx and the epoxide molecules. We conducted a systematic examination of how the degree of polymerization and the nature of grafted epoxide molecules influence mRNA delivery efficiency. *In vitro* experiments demonstrated that DP50-PE6, synthesized *via* a ring-opening reaction between 1,2-epoxydecane (E6) and $PAmOx_{50}$, enhanced mRNA transfection efficiency by a staggering 3.3×10^5-fold compared with the parent $PAmOx_{50}$. Consistent with the *in vitro* findings, *in vivo* intramuscular administration of the DP50-PE6/mRNA complex exhibited robust expression at the site of injection (1.8×10^6 p/sec/cm^2/sr) and remained detectable for two days. Notably, following intravenous administration, the DP50-PE6/mRNA complex exhibited selective protein expression in the spleen which accounted for approximately 85.1% of the total expression observed across major organs. Further research revealed that the DP50-PE6/mOVA complex, when combined with anti-PD1, effectively inhibited tumor growth in the B16-OVA melanoma model, achieving a tumor suppression rate over 90%. These findings underscore the immense potential of POx-based vectors in mRNA delivery, setting the stage for the evolution of POx-inspired nucleic acid delivery vectors.

Received 30th June 2025
Accepted 25th September 2025

DOI: 10.1039/d5sc04801j

rsc.li/chemical-science

Introduction

Messenger RNA (mRNA) technology has revolutionized the landscape of genetic medicine, offering a versatile and potent approach for vaccine development, protein replacement therapies, and cancer immunotherapy.[1–4] The clinical success of mRNA vaccines, exemplified by the FDA-approved Pfizer-BioNTech and Moderna COVID-19 vaccines, has underscored the immense potential of mRNA-based therapeutics.[5,6] However, realizing the full therapeutic promise of mRNA necessitates the development of efficient delivery systems that can ensure intracellular mRNA stability, facilitate cytoplasmic release, and enable precise organ targeting.[7–9] Naked mRNA suffers from inherent limitations, including rapid degradation by nucleases, low cellular uptake, and undesired immunogenicity.[10–13] Consequently, the design of an optimal mRNA delivery system must address key challenges including improving transfection efficiency, enhancing stability, achieving organ selectivity, and maintaining biocompatibility.[14–18]

Lipid nanoparticles (LNPs) have emerged as the leading mRNA delivery platform due to their high transfection efficiency and clinically validated performance.[19–22] Comprising ionizable lipids, helper phospholipids, cholesterol, and polyethylene glycol (PEG)-lipids, LNPs protect mRNA from enzymatic degradation and promote efficient cellular uptake.[23] Despite their success, LNPs present certain drawbacks, including instability, liver tropism, limited biodegradability, and restricted versatility in targeting extrahepatic organs.[12,24–26] In contrast, polymer-based delivery systems offer an attractive alternative with improved structural stability, tunable chemical properties, favorable biocompatibility and the potential for controlled organ distribution.[27–30] However, the relatively low transfection efficiency of polymeric carriers remains a major hurdle, necessitating further structural optimization.[31,32]

[a]*State Key Laboratory of Polymer Science and Technology, Changchun Institute of Applied Chemistry, Chinese Academy of Sciences, Changchun 130022, China. E-mail: wtsong@ciac.ac.cn*

[b]*School of Applied Chemistry and Engineering, University of Science and Technology of China, Hefei 230026, China*

[c]*Jilin Biomedical Polymers Engineering Laboratory, Changchun 130022, China*

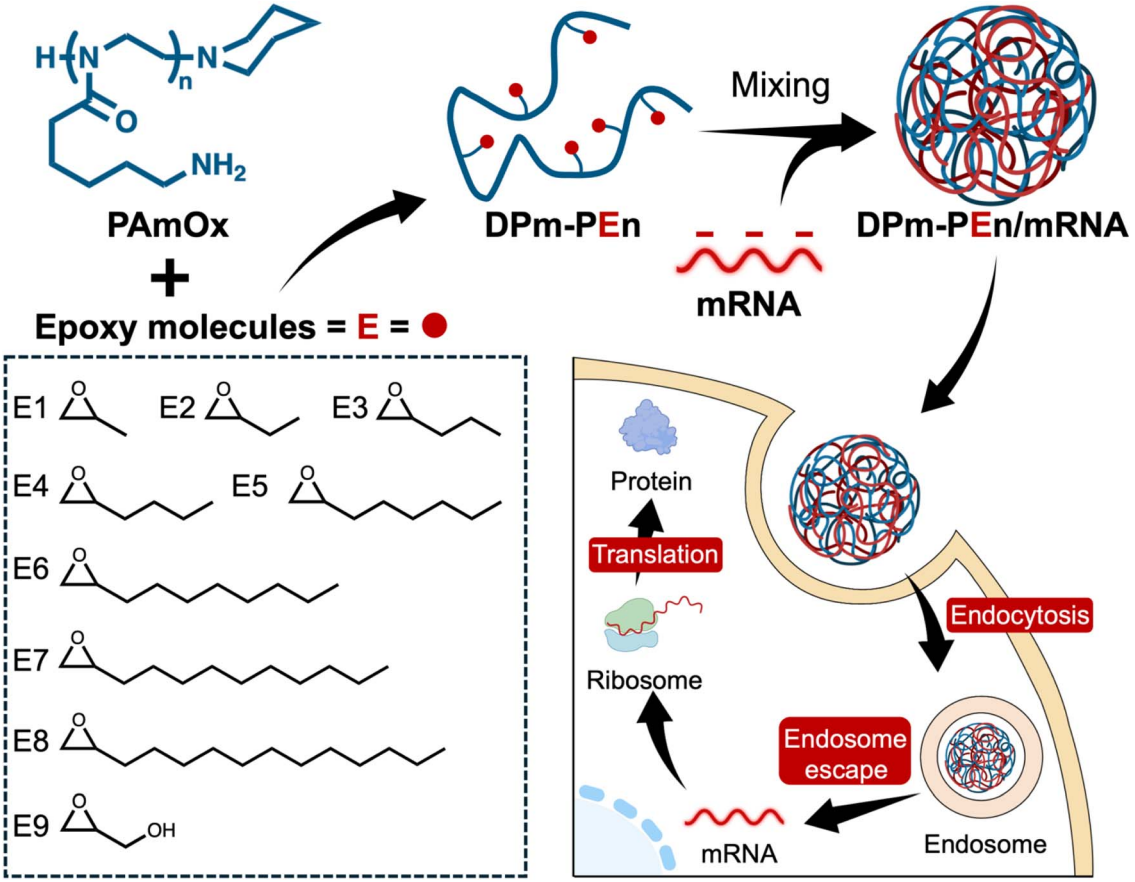

Fig. 1 Schematic illustration of the POx-based carrier (DPm-PEn) design and the mechanism of mRNA delivery to cells. Abbreviations for epoxy molecules shown in the figure: propylene oxide (E1), 1,2-epoxybutane (E2), 1,2-epoxypentane (E3), 1,2-epoxyhexane (E4), 1,2-epoxyoctane (E5), 1,2-epoxydecane (E6), 1,2-epoxydodecane (E7), 1,2-epoxytetradecane (E8), glycidol (E9).

Poly(2-oxazoline)s (POx) have garnered significant attention in biomedical applications due to their tunable physicochemical properties, biocompatibility, and ease of functionalization.[33–36] Recent studies have begun to explore POx for mRNA delivery, for instance, by leveraging it as a PEG substitute in LNP formulations or by using cationic POx for the delivery of self-amplifying RNA (saRNA).[37–40] However, systematic studies on the rational design of cationic POx as delivery vectors for conventional mRNA, especially for applications like cancer vaccination, remain limited. Interestingly, linear polyethyleneimine (LPEI), as a hydrolyzed product of POx, is the most widely studied cationic polymer in the field of mRNA delivery.[41–43] Its strong electrostatic interaction with mRNA makes LPEI a promising candidate for mRNA delivery, ensuring efficient complex formation and cellular uptake.[44] However, PEI's high cationic density results in cytotoxicity that limits its further *in vivo* application.[45,46] We hypothesize that POx can achieve efficient mRNA delivery with good biosafety through the rational design of side-chain structure.

In this study, we developed a simple one-step post-modification approach to construct a series of POx-based mRNA delivery vectors with enhanced transfection efficiency and organ-targeting capabilities. Poly[2-(5-aminopentyl)-2-oxazoline] (PAmOx) was reacted with various epoxide molecules through ring-opening reactions to obtain DPm-PEn (Fig. 1). DP25-PE6 and DP50-PE6 were selected based on their well-performed *in vitro* transfection capabilities. The protein expression mediated by these selected polymers exceeded 10^{10} RLU per mg protein. Following intramuscular injection, DP25-PE6 and DP50-PE6 enabled high local protein expression at the injection site. Intravenous administration of DP50-PE6 resulted in predominant protein expression in the spleen, accounting for 85.1% of the total expression across major organs, indicating strong spleen-targeting potential. To evaluate its therapeutic potential, DP50-PE6 was further tested in a B16-OVA melanoma model. Remarkably, DP50-PE6 elicited a robust antigen-specific immune response and achieved substantial tumor growth inhibition, with a tumor suppression rate (TSR%) of 90%. These results underscore the versatility and efficacy of DPm-PEn as a kind of potent mRNA delivery vectors.

Results and discussion

Rational design and synthesis of DPm-PEn

Amino-functionalized PAmOx was selected as the starting material due to its inherent cationic properties, which allow for efficient electrostatic interaction and loading of mRNA. To further enhance its cellular uptake and endosomal escape

capacity, we modified the side chains of PAmOx by reacting the amino groups with epoxides containing varying alkyl chains.[47] This straightforward one-step strategy resulted in the generation of a diverse library of DPm-PEn conjugates with distinct hydrophobic properties, enabling a screening process to identify optimal candidates for mRNA delivery.

To achieve this design, 2-oxazoline monomer with Boc-protected amino group was synthesized from 6-(Boc-amino) caproic acid[48] and then polymerized using trimethylsilyl trifluoromethanesulfonate (TMSOTf) as the initiator to afford PBoc-AmOx[49] (Schemes S1, S2 and S1–S5). Polymers with target degrees of polymerization (DP) of 25, 50, 75 and 100 were synthesized by adjusting the feeding ratios of monomer and initiator, and the actual DPs were measured to be 24, 50, 78 and 96, respectively (Fig. S2–S5, ^{1}H NMR spectra). The obtained PBoc-AmOx was further characterized using gel permeation chromatography (GPC). The number-average molecular weight (M_n) of the representative PBoc-AmOx$_{50}$ was determined to be 12.5 kDa, with a polymer dispersity index (PDI) of 1.2 (Fig. S6). After removing the N-Boc protecting group, a series of epoxy-functionalized POx (DPm-PEn, m = 25, 50, 75 or 100; n = 1–9) were obtained by ring–opening reactions of PAmOx of different DPs with nine different epoxide molecules (Fig. 1, S7 and Scheme S3).[50] The appearance of peak 'Ha' (–CH_3) in the ^{1}H NMR spectra confirmed the successful ring–opening reaction between the PAmOx and the epoxide molecules (Fig. S8). The grafting efficiencies of the individual polymers, determined from the integration of characteristic ^{1}H NMR peaks, are summarized in Table S1. This process yields a series of polymers with different DPs and hydrophobic chains. Subsets of this library were termed DPm-PEn (m = 25, 50, 75 or 100; n = 1–9), depending on the combination of different DP and En. Utilizing this simple one-step post-modification process, we designed an expandable library of POx-based mRNA delivery vectors with diverse chemical structures.

In vitro transfection efficiency and cytotoxicity

The transfection efficiency is closely linked to the chemical structure of the mRNA delivery vector.[51–53] To explore the structure-activity relationships (SAR) of polymeric vectors, DPm-PEn were used to deliver mRNA encoding firefly luciferase (Fluc) to 293T cells. In preliminary study, cationic DPm-PEn polymers were complexed with mRNA at a polymer-to-mRNA mass ratio of 30/1 to form polyplexes (Fig. 2a), with the corresponding N/P ratios for each polymer detailed in Table S2. In the *in vitro* screening heat maps (Fig. 2b), we observed that PAmOx were initially devoid of any transfection efficacy. Upon reaction with E5, E6, or E7, it transformed into a functionalized polymer with enhanced transfection efficiency. This indicates that the introduction of hydrophobic alkyl chains is crucial for mRNA delivery.[54,55] Among all tested polymers, DP50-PE6 exhibited the highest *in vitro* transfection efficiency, which was 3.3 × 10^5 times greater than that of PAmOx$_{50}$ (Fig. 2c). This finding highlights the importance of optimizing both the DP and alkyl chain length to maximize the delivery potential of cationic polymer-based mRNA carriers.

The transfection efficiency of DP100-PE6 was significantly lower than that of DP50-PE6. This may be caused by the higher DP of DP100-PE6, which could lead to stronger cytotoxicity, thus affecting cell viability and transfection efficiency. We conducted an experiment to assess the cytotoxicity of DPm-PEn using 293T cells (Fig. 3a). It was found that the cell viability of PAmOx was merely 20%. Upon grafting with E2, E3, and E4 molecules, the cell viability of the polymer increased slightly, yet remained within a limited range of 20% to 40%. Interestingly, when grafted with E1, E5, E6, E7, E8, and E9 molecules, the cell viability of the polymer significantly improved, reaching 30% to 100% (Fig. 3b, c and S9). This seemingly counterintuitive trend, where longer hydrophobic chains led to lower cytotoxicity, can be attributed to the polymer's state. When evaluated alone, using the DP25 series of polymers as a representative example, the excessively hydrophobic E5–E7 polymers exhibited poor aqueous solubility and precipitated during preparation, which limited their bioavailability and capped their apparent cytotoxicity (Fig. S10). Upon complexation with mRNA, however, their strong hydrophobic interactions became advantageous, driving the formation of compact polyplexes (Fig. S11). This structure effectively sequesters the membrane-disruptive hydrophobic chains internally. In contrast, the weaker hydrophobicity of the E2–E4 series was insufficient for complete shielding, leaving cytotoxic domains exposed on the polyplex surface. Therefore, the superior cytocompatibility of the E5–E7 series is a direct consequence of this structurally enforced shielding upon polyplex formation. While all DPm-PE6/PE7 polymers demonstrated superior transfection efficiency *in vitro*, their cytotoxicity profiles varied with DP. At DP 25, negligible toxicity was observed, indicating a viable window for low-DP formulations. However, escalating DP led to progressive cytotoxicity, culminating in nearly 40% cell death at DP 100, potentially attributable to increased polymer-cell membrane interactions. Furthermore, 293T cells were treated with PAmOx$_{25}$, DP25-PE6, DP50-PE6, DP75-PE6, and DP100-PE6, followed by staining with Calcein-AM and PI. As shown in Fig. 3d, treatment with PAmOx$_{25}$ resulted in almost complete loss of green fluorescence, indicating a high level of cytotoxicity and poor cell viability. In contrast, all E6-grafted polymers showed markedly improved biocompatibility, with strong green fluorescence and minimal red fluorescence observed. Evidently, as the DP increased, green fluorescence decreased significantly while red fluorescence intensified, further substantiating that cytotoxicity rises in correlation with the increase in the DP. These results suggested that an appropriate alkyl chain length, as well as the DP, was beneficial to maintain the balance between efficient mRNA delivery and low toxicity. By optimizing these two parameters, we can design polymers with high transfection efficiency and low cytotoxicity, which are suitable for *in vivo* applications.

Next, we investigated the effect of the polymer-to-mRNA mass ratio on transfection efficiency. According to the data presented in Fig. 2c, polymers exhibiting Fluc fluorescence intensity greater than 1.0 × 10^9 RLU per mg were selected as representative candidates, including DP25-PE6, DP25-PE7, DP50-PE6, DP50-PE7, DP75-PE6, DP75-PE7, DP100-PE6, and

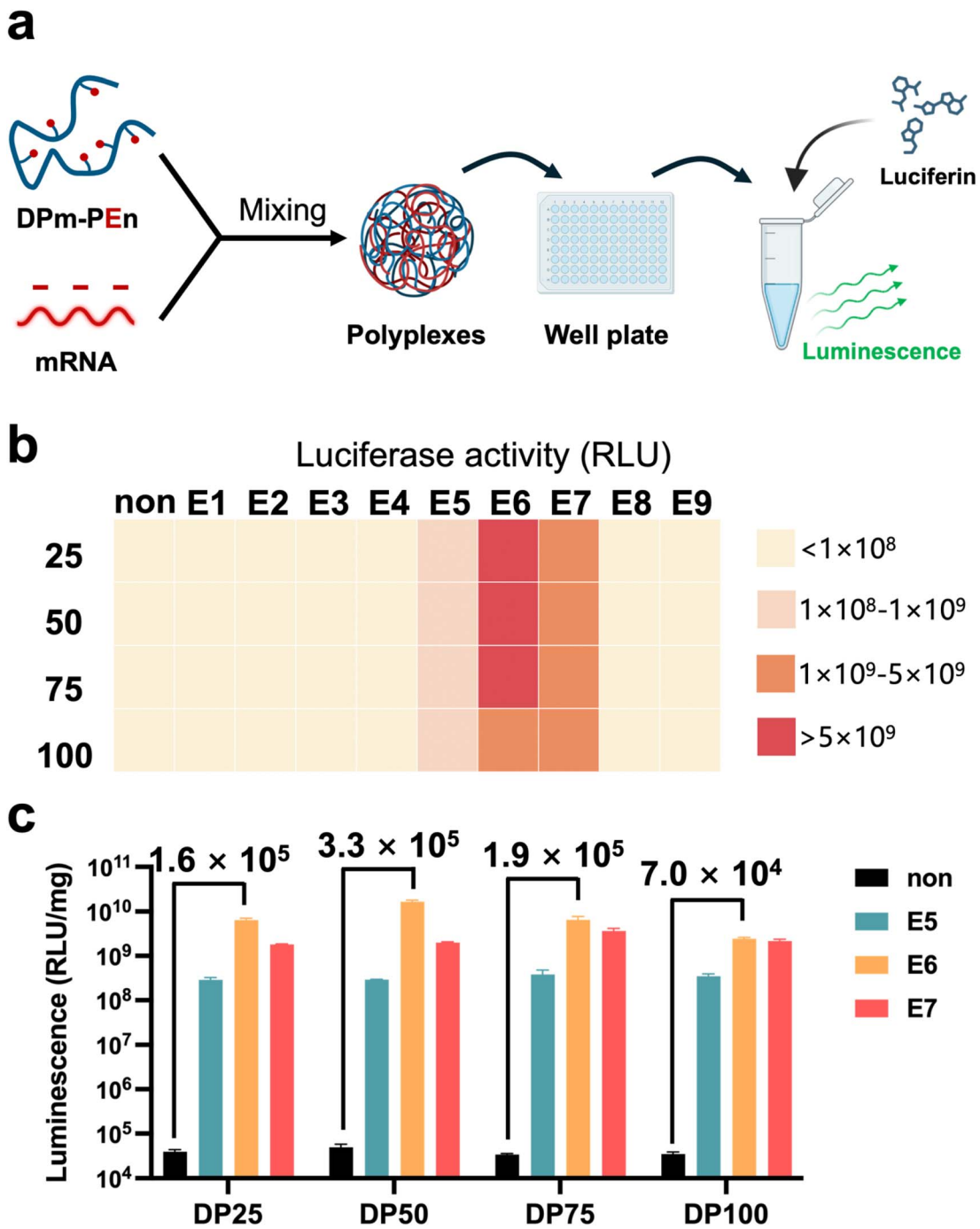

Fig. 2 *In vitro* screening of DPm-PEn polymers for mRNA transfection in 293T cells. (a) Schematic illustration of the evaluation of *in vitro* mRNA delivery efficiency. (b) Evaluation of DPm-PEn *in vitro* delivery of Fluc mRNA (200 ng per well) in 293T cells, with fluorescence intensity assessed after 24 hours of incubation. (c) The relationship between the type of grafted epoxide molecules and transfection efficiency. The data are presented as mean ± s.d. ($n = 3$).

DP100-PE7. The mass ratios of polymer to mRNA were systematically varied at 1 : 1, 5 : 1, 15 : 1, and 30 : 1, with their corresponding N/P ratios detailed in Table S3. The results revealed a distinct trend, where transfection efficiency initially increased with the mass ratio, reaching a peak, and then declined at higher polymer-to-mRNA mass ratios (Fig. 4). Interestingly, 60% of the polymers demonstrated optimal transfection efficiency at a polymer-to-mRNA mass ratio of 15 : 1. Notably, at this ratio, DP25-PE6 and DP50-PE6 exhibited the most efficient mRNA delivery. These findings highlight the critical importance of fine-tuning the polymer-to-mRNA mass ratio in order to maximize transfection efficiency. Based on these results, we selected two polymers, DP25-PE6 and DP50-PE6, with a fixed polymer-to-mRNA mass ratio of 15 : 1 for subsequent investigations.

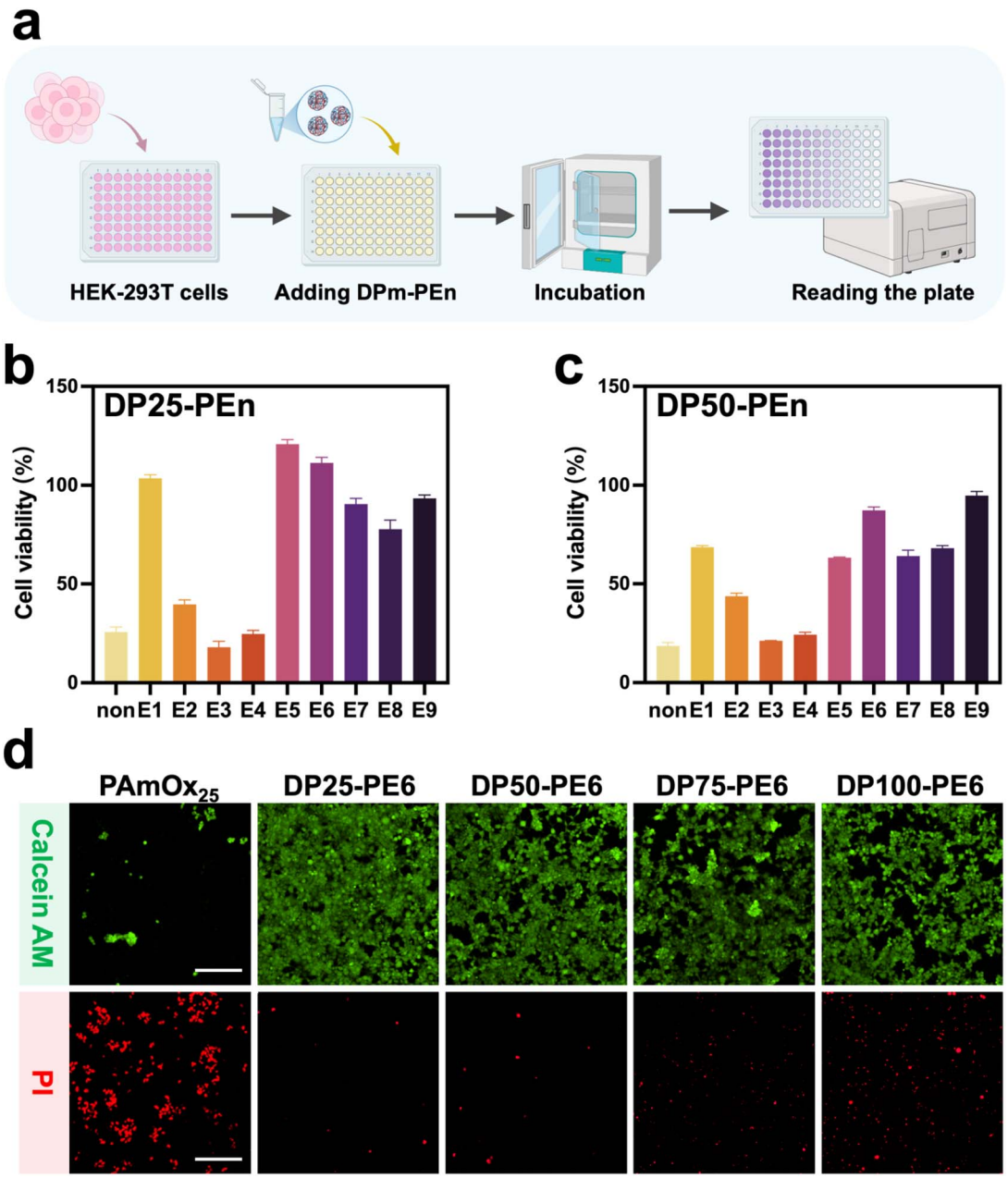

Fig. 3 *In vitro* safety assessment of DPm-PEn/mRNA polyplexes in 293T cells. (a) Schematic illustration of the evaluation of *in vitro* cell viability. (b and c) Cell viability of DP25-PEn (b) and DP50-PEn (c) mRNA polyplexes. (d) Live (green)/dead (red) fluorescence results of $PAmOx_{25}$, DP25-PE6, DP50-PE6, DP75-PE6 and DP100-PE6 (scale bar = 200 μm). The data are presented as mean ± s.d. (n = 3).

Stability, mRNA transfection across cell lines, and serum resistance

Nanoparticles formed by compounding polymers with mRNA were firstly characterized by dynamic light scattering (DLS) to assess the materials' ability to condense mRNA. The size of the nanoparticles formed with DP25-PE6 was 175 nm with a polydispersity index (PDI) of 0.13, while the size of DP50-PE6 was 162 nm with a PDI of 0.258 (Fig. 5a and d). These results indicate that both materials effectively self-assemble with mRNA to form stable nanoparticles. Next, the stability of the nanoparticles over time was evaluated, as it is a key factor for efficient mRNA delivery. We monitored the particle size of the nanoparticles formed by both DP25-PE6 and DP50-PE6 at 0, 1, 2, 4, and 8 days post-formation (Fig. 5b and e). Nanoparticles formed by DP50-PE6 exhibited size stability throughout the observation period. However, the nanoparticles formed by DP25-PE6 showed a significant increase in particle size over time. This could be attributed to its lower DP, which might not effectively condense the mRNA, thereby leading to instability of the nanoparticles. Additionally, the stability and functional integrity of the polymers in ambient conditions were examined. The polymers were stored at room temperature for 0, 1, 2, 4, and 8

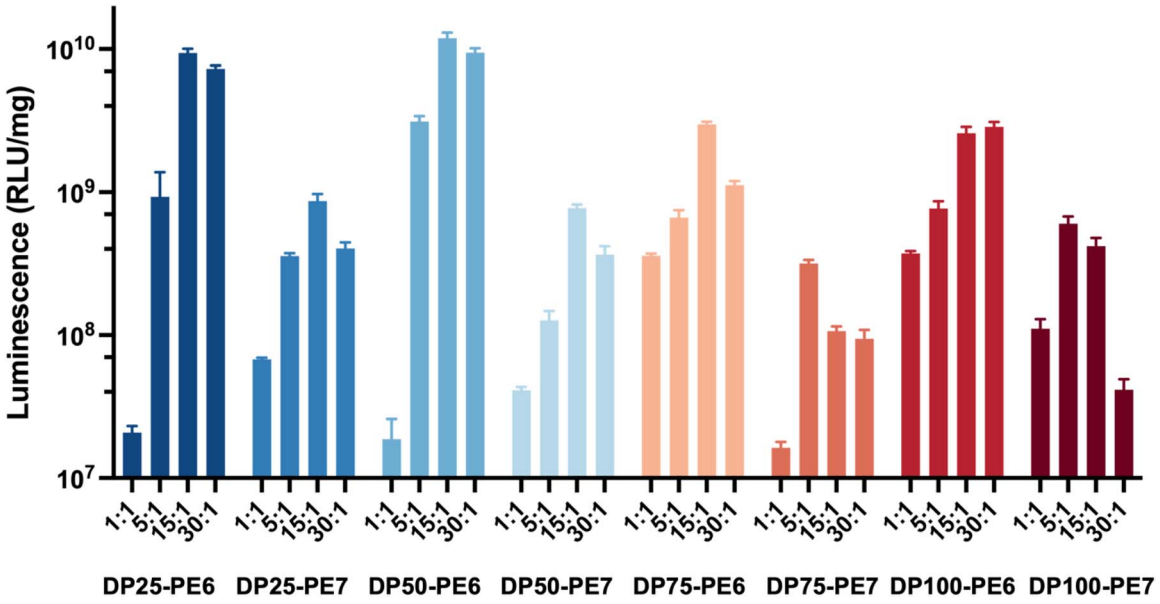

Fig. 4 Transfection efficiency of DP25-PE6, DP25-PE7, DP50-PE6, DP50-PE7, DP75-PE6, DP75-PE7, DP100-PE6 and DP100-PE7 in 293T cells at various mass ratios (polymer/mRNA = 1 : 1, 5 : 1, 15 : 1, and 30 : 1). The data are presented as mean ± s.d. ($n = 3$).

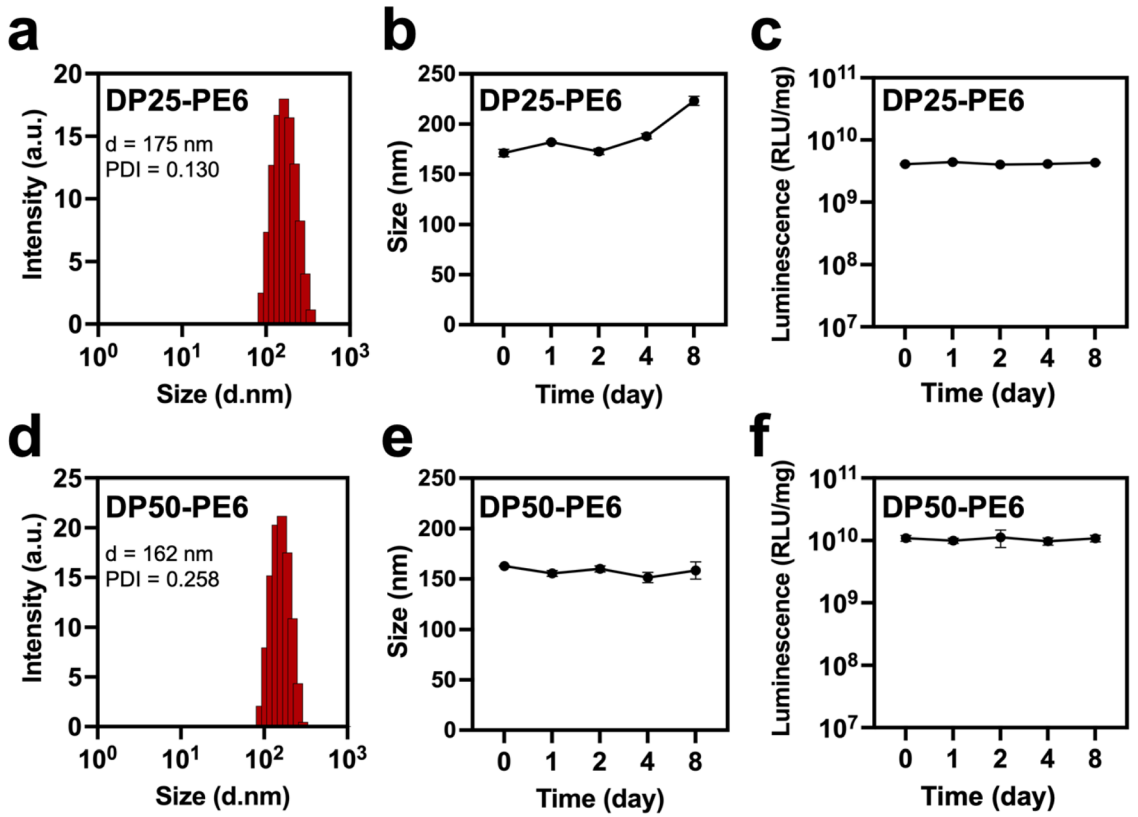

Fig. 5 Particle size and stability of DP25-PE6 and DP50-PE6 mRNA polyplexes. (a) DLS measurement of DP25-PE6/mRNA polyplexes. (b) DLS analysis of DP25-PE6/mRNA polyplexes to assess particle size stability over time (0, 1, 2, 4, and 8 days). (c) Evaluation of transfection efficiency of DP25-PE6 in 293T cells following storage for different time periods (0, 1, 2, 4, and 8 days). (d) DLS measurement of DP50-PE6/mRNA polyplexes. (e) DLS analysis of DP50-PE6/mRNA polyplexes to assess particle size stability over time (0, 1, 2, 4, and 8 days). (f) Evaluation of transfection efficiency of DP50-PE6 in 293T cells following storage for different time periods (0, 1, 2, 4, and 8 days). The data are presented as mean ± s.d. ($n = 3$).

days and their mRNA delivery efficiency was assessed on 293T cells. The results demonstrated that both DP25-PE6 and DP50-PE6 maintained high mRNA delivery efficiency regardless of the storage duration, underscoring the robustness and stability of these polymers under ambient conditions (Fig. 5c and f).

We further evaluated the transfection efficiency of DP25-PE6 and DP50-PE6 across a range of cell types, including fibroblasts, immune cells, and tumor cells. Both polymers exhibited robust mRNA delivery, achieving Fluc fluorescence intensities exceeding 10^8 RLU per mg across all tested cell lines (Fig. 6a). Compared with the benchmark polymer LPEI, the transfection efficiency of DP25-PE6 and DP50-PE6 increased by one to two orders of magnitude (Fig. S12). Notably, the transfection efficiency was particularly high in DC2.4 cells, with Fluc fluorescence intensities surpassing 10^9 RLU per mg for both DP25-PE6 and DP50-PE6. Dendritic cell (DC) is a key antigen-presenting cell (APC) that plays a critical role in immune response initiation. The exceptional transfection efficiency in these cells highlights the potential of DPm-PEn for mRNA vaccine delivery. These findings collectively demonstrate that DPm-PEn, particularly DP25-PE6 and DP50-PE6, are highly effective for mRNA delivery across a broad range of cell types.

To investigate the internalization mechanism of DPm-PE6/mRNA polyplexes, 293T cells were pretreated with a series of endocytic inhibitors. Chlorpromazine (CPZ), a known inhibitor of clathrin-mediated endocytosis, led to an approximately 10–

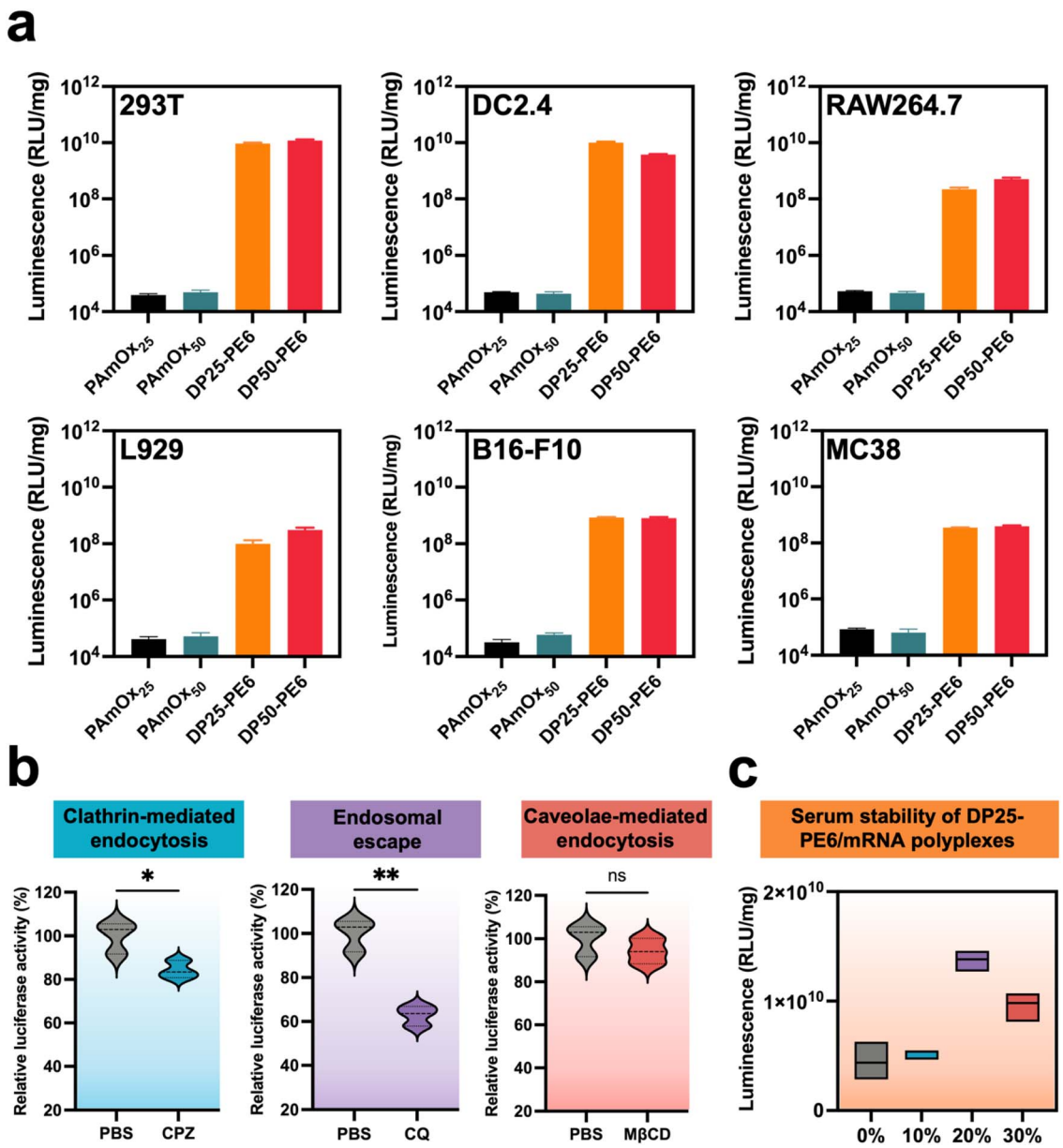

Fig. 6 (a) Transfection efficiency of DP25-PE6 and DP50-PE6 mRNA polyplexes in 293T, DC2.4, RAW264.7, L929, B16–F10, and MC38 cells. (b) Effects of inhibitors on cellular uptake and endosomal escape of DP25-PE6/mRNA polyplexes. (c) Transfection efficiency of DP25-PE6/mRNA polyplexes in 293T cells under varying FBS concentrations (0%, 10%, 20%, and 30%). The data are presented as mean ± s.d. ($n = 3$). (ns: not significant, *$p < 0.05$, **$p < 0.01$).

20% reduction in luminescence intensity associated with DP25-PE6 and DP50-PE6, suggesting the participation of clathrin-dependent pathways in polyplex uptake (Fig. 6b and S13). In addition, treatment with chloroquine (CQ), which disrupts endosomal acidification, resulted in an approximately 40% decrease in mRNA transfection efficiency, underscoring the critical role of endosomal escape for successful mRNA delivery. We next investigated the mRNA delivery efficiency across a range of fetal bovine serum (FBS) concentrations. This experiment aimed to simulate the conditions of biological fluids and assess the impact of serum proteins on the polyplexes' stability and transfection efficiency. The results demonstrated that the mRNA delivery efficiencies of both DP25-PE6 and DP50-PE6 exhibited a concentration-dependent trend, first increasing and then decreasing with the rising FBS concentration (Fig. 6c and S14). Notably, DP25-PE6 exhibited the highest mRNA transfection efficiency at 20% FBS, while DP50-PE6 reached its peak transfection efficiency at 10% FBS. Overall, these results indicate that DPm-PEn exhibit favorable serum stability, which is crucial for their potential use in *in vivo* applications.

In vivo study of DPm-PEn for mRNA delivery

In the next stage, DP25-PE6 and DP50-PE6 were selected to evaluate the *in vivo* mRNA delivery efficiency. For the intramuscular administration, DPm-PEn/mRNA polyplexes were

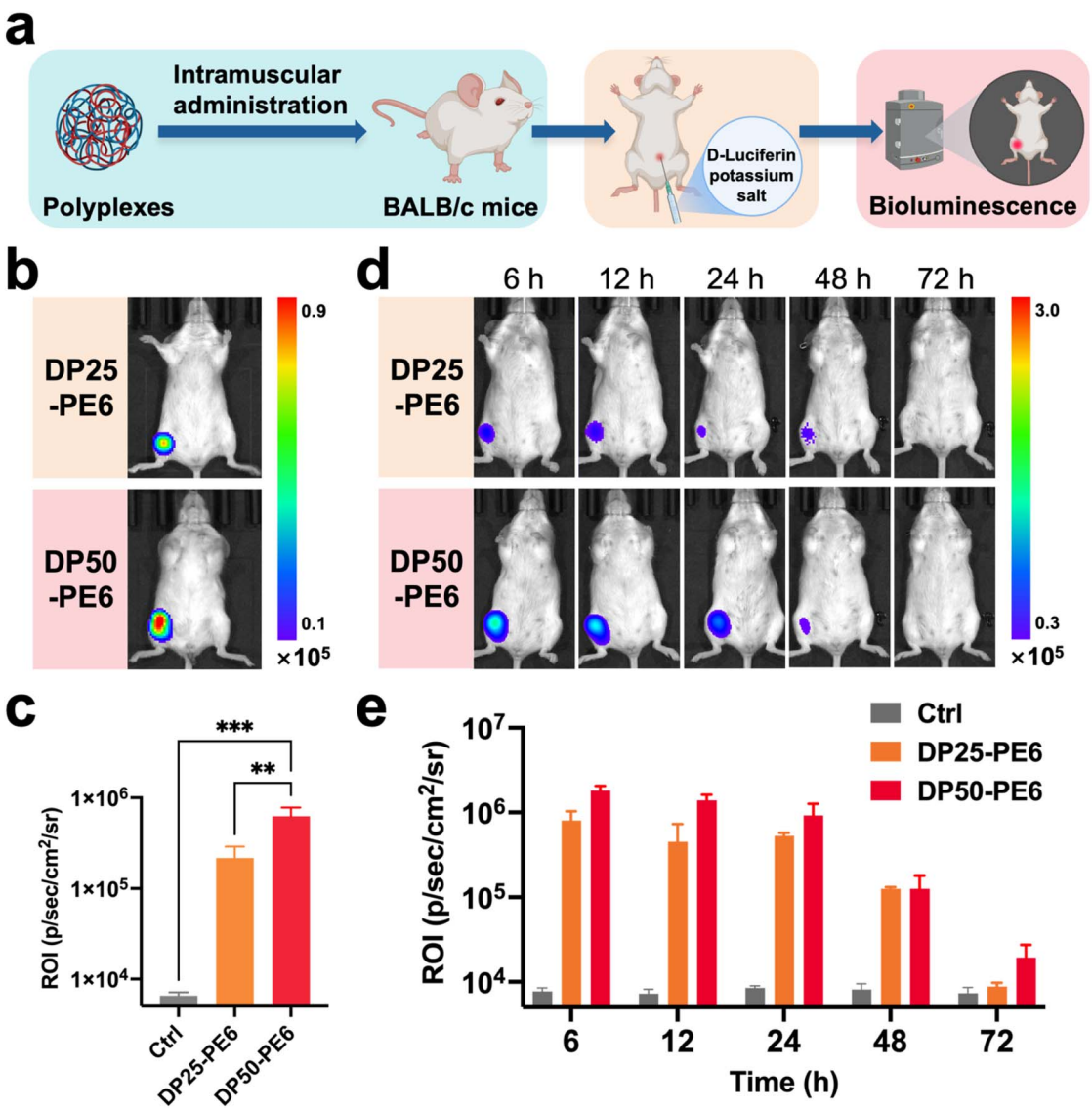

Fig. 7 *In vivo* mRNA transfection efficiency of DP25-PE6 and DP50-PE6 mFluc polyplexes following intramuscular injection. (a) The scheme of *in vivo* transfection experiments. The intramuscular administration of the DPm-PEn/mRNA polyplexes was at a dose of 0.25 mg kg^{-1}. (b) Bioluminescence images of mice 24 hours after intramuscular injection of DP25-PE6 and DP50-PE6 mFluc polyplexes. (c) Quantification of Fluc protein expression by DP25-PE6 and DP50-PE6 mFluc polyplexes. (d) Bioluminescence images acquired at 6 h, 12 h, 24 h, 48 h, and 72 h following intramuscular administration of DP25-PE6 and DP50-PE6 mFluc polyplexes. (e) Quantification of Fluc protein expression at 6, 12, 24, 48, and 72 hours after intramuscular injection of DP25-PE6 and DP50-PE6 mFluc polyplexes. The data are presented as mean ± s.d. ($n = 3$). (ns: not significant, *$p < 0.05$, **$p < 0.01$, ***$p < 0.001$).

injected into mice at a dose of 0.25 mg kg^{-1}. After 24 hours, the luciferase substrate, D-Luciferin potassium salt, was administered, and firefly luciferase expression was quantified by measuring the total luminescent flux at the injection site (Fig. 7a). Both DP25-PE6 and DP50-PE6 proved effective in mediating luciferase expression at the injection site (Fig. 7b and c). Compared with the benchmark LPEI and DP25-PE6, DP50-PE6 increased luciferase expression by 3-fold in both cases (Fig. S15). This result is consistent with *in vitro* findings and affirms the superiority of DP50-PE6 for efficient local mRNA

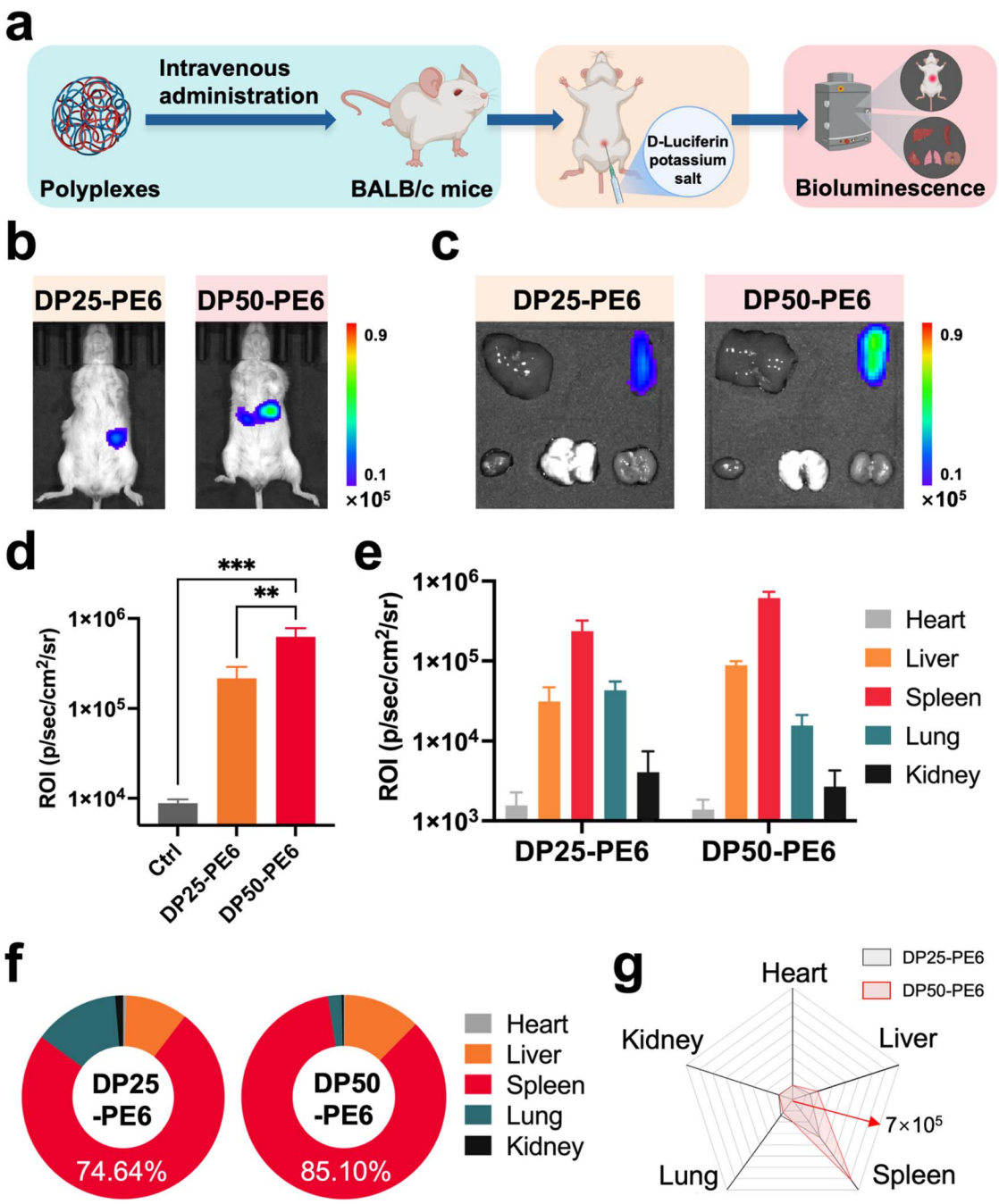

Fig. 8 *In vivo* mRNA transfection efficiency of DP25-PE6 and DP50-PE6 mFluc polyplexes at 24 hours after intravenous injection. (a) The scheme of *in vivo* transfection experiments. The intravenous administration of the DPm-PEn/mRNA polyplexes was at a dose of 0.25 mg kg^{-1}. (b) Bioluminescence images of mice 24 hours after intravenous injection of DP25-PE6 and DP50-PE6 mFluc polyplexes. (c) Bioluminescence images of main organs (heart, liver, spleen, lungs, and kidneys) collected 24 hours post intravenous administration of DP25-PE6 and DP50-PE6 mFluc polyplexes. (d) Quantification of Fluc protein expression by DP25-PE6 and DP50-PE6 mRNA polyplexes. (e) Quantification of Fluc protein expression by DP25-PE6 and DP50-PE6 mRNA polyplexes in major organs. (f) Percentage of total Fluc protein expression mediated *via* DP25-PE6 and DP50-PE6 in the main organs. (g) The quantitative analysis of Fluc protein expression in the spleen showed organ-specific distribution and expression levels. The data are presented as mean ± s.d. ($n = 3$). (ns: not significant, *$p < 0.05$, **$p < 0.01$, ***$p < 0.001$).

delivery. As the duration of mRNA expression is critical for the efficacy of mRNA vaccines, we assessed the sustained expression of firefly luciferase at various time points: 6, 12, 24, 48, and 72 hours post-injection. Both DP25-PE6 and DP50-PE6 sustained luciferase expression for up to 48 hours (Fig. 7d and e).

Encouraged by the robust luciferase expression observed after intramuscular injection, we next sought to evaluate *in vivo* mRNA delivery efficiency of DP25-PE6 and DP50-PE6 *via* intravenous (*i.v.*) administration. DPm-PEn/mRNA polyplexes were injected into BALB/c mice through the tail vein at a dose of 0.25 mg kg^{-1}. After 24 hours, D-Luciferin potassium salt was administered by intraperitoneal (*i.p.*) injection, and *in vivo* bioluminescence imaging was performed to assess firefly luciferase expression (Fig. 8a). Both polyplexes showed efficient luciferase expression, with DP50-PE6 mediating higher expression levels than DP25-PE6—consistent with the results from intramuscular delivery (Fig. 8b and d). Most notably, the luciferase expression level mediated by DP50-PE6 was a remarkable 28-fold higher than that of the benchmark LPEI (Fig. S16). To further pinpoint the site of protein expression, major organs

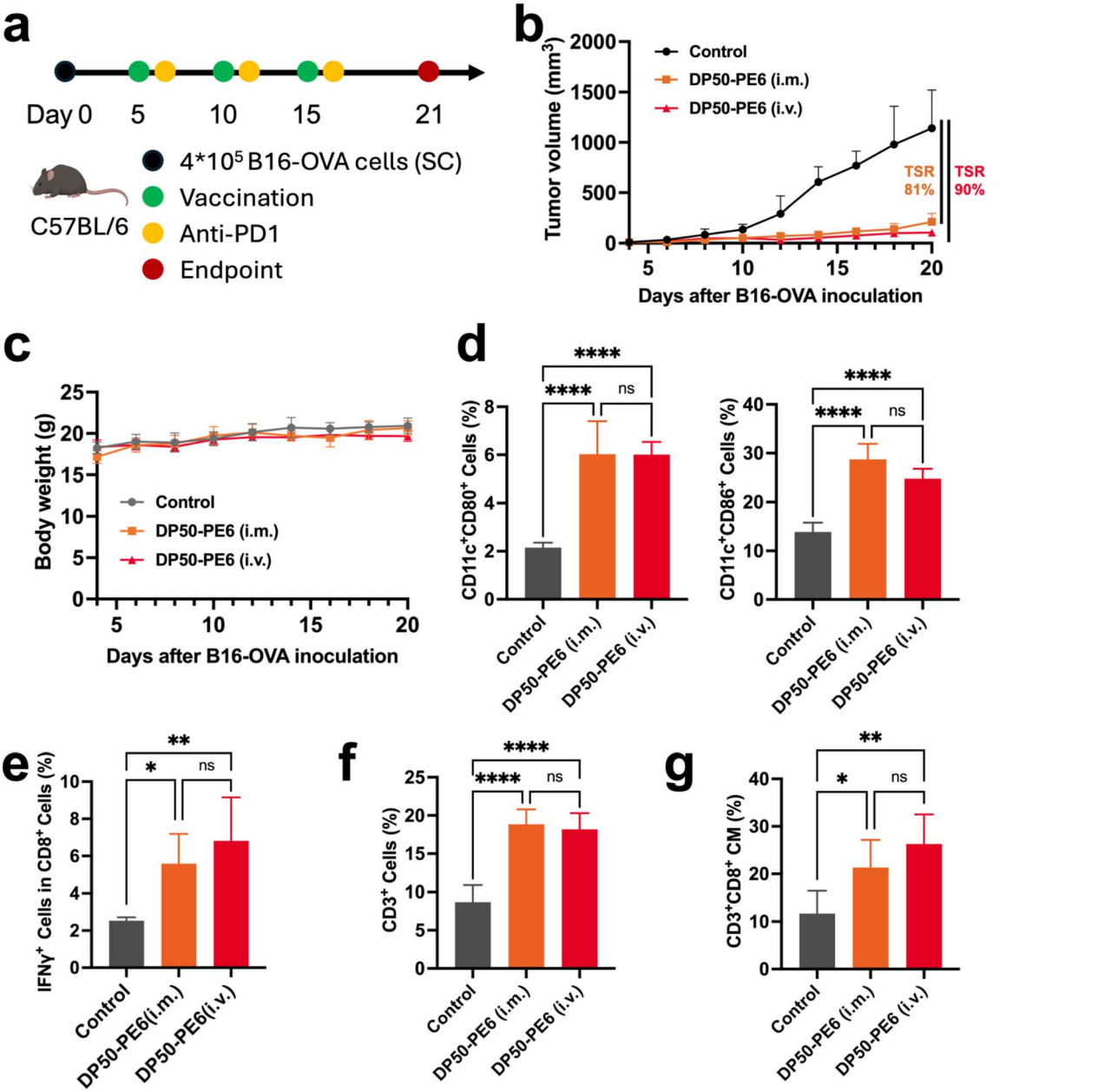

Fig. 9 (a) Schematic illustration of tumor inoculation and treatment schedule. (b) Average tumor growth curves of mice in different treatment groups ($n = 5$). (c) The body weight changes of B16-OVA tumor-bearing mice in different treatment groups ($n = 5$). (d) The percentage of $CD11c^+CD80^+$ cells and $CD11c^+CD86^+$ cells within the lymph nodes on day 21. (e) FACS analysis of IFN-γ positive T cells in the peripheral blood on day 20. (f) The percentage of $CD3^+$ cells within the tumor on day 21. (g) The percentage of $CD3^+CD8^+$ CM cells within the spleen on day 21. The data are presented as mean ± s.d. ($n = 3$). (ns: not significant, *$p < 0.05$, **$p < 0.01$, ***$p < 0.001$, ****$p < 0.0001$).

including the heart, liver, spleen, lungs, and kidneys were harvested for *ex vivo* imaging (Fig. 8a). Interestingly, luciferase expression was predominantly enriched in the spleen, suggesting a unique spleen-targeting property of the DPm-PEn carrier (Fig. 8c and e). Quantitative analysis revealed that DP50-PE6 mediated 85.1% of the total protein expression in the spleen, indicating a strong organ preference (Fig. 8f). This spleen-selective protein expression profile is particularly attractive for vaccine applications where efficient delivery to immune-related organs is required. Between the two polymers, DP50-PE6 exhibited significantly superior spleen-targeted delivery, reinforcing its potential as a systemic mRNA vaccine carrier (Fig. 8g).

Therapeutic evaluation in B16-OVA tumor model

Building on the efficient mRNA delivery performance of DP50-PE6 observed *via* both *i.m.* and *i.v.* administration, we further evaluated its potential as a vaccine vector for cancer immunotherapy. A B16-OVA tumor model was established by subcutaneously injecting 4×10^5 B16-OVA cells into the right flank of C57BL/6 mice on day 0. Mice were then randomly assigned into three groups: (1) control (PBS, *i.v.*; anti-PD-1, *i.p.*), (2) DP50-PE6 (*i.m.*), and (3) DP50-PE6 (*i.v.*). The respective treatments (PBS or DP50-PE6/mOVA) were administered on days 5, 10, and 15. Subsequently, all groups received an intraperitoneal injection of anti-PD-1 antibody on days 6, 11, and 16 (Fig. 9a). Notably, both *i.m.* and *i.v.* administration of DP50-PE6/mOVA (full-length ovalbumin-encoding mRNA) significantly suppressed tumor growth compared to the Control group. The TSR% reached approximately 90% in DP50-PE6 (*i.v.*) group (Fig. 9b). This underscores the robust therapeutic efficacy of DP50-PE6 as an mRNA vaccine carrier. Moreover, there were no significant changes in body weight across any groups during the observation period, suggesting good biocompatibility and minimal systemic toxicity with these treatment regimens (Fig. 9c).

On day 21, mice were sacrificed, and blood, spleens, lymph nodes, and tumors were collected for immunological analysis. To assess the immune activation triggered by the vaccine, DCs in the lymph nodes were first analyzed by flow cytometry. Compared to the Control group, both *i.m.* and *i.v.* administration of DP50-PE6/mOVA led to a significant upregulation in the expression of costimulatory molecules CD80 and CD86 (Fig. 9d and S17). This suggests effective activation and maturation of DCs within the lymph nodes. Further analysis of DCs within the tumor microenvironment revealed a consistent pattern (Fig. S18 and S19). In the vaccine-treated groups, there was a marked increase in the expression of DC costimulatory molecules relative to the Control group, demonstrating that DP50-PE6/mOVA also enhances DC activation within tumors. We then evaluated T cell responses in the peripheral blood. Flow cytometric analysis revealed a significant elevation in the proportion of IFN-γ^+ $CD8^+$ T cells in both the *i.m.* and *i.v.* vaccinated groups compared to the Control group, signaling robust activation of cytotoxic T cell responses, which is in line with the observed anti-tumor efficacy (Fig. 9e and S20). Furthermore, we evaluated T cell infiltration within the tumor tissue. Both administration routes of DP50-PE6/mOVA resulted in a substantial increase in tumor-infiltrating T cells compared with the Control group (Fig. 9f and S21). Finally, to assess the induction of immune memory, we analyzed memory T cell populations in the spleen following multiple vaccinations. A noteworthy increase in $CD8^+$ central memory T cells was evident in the vaccine-treated groups compared to the Control group, suggesting that DP50-PE6/mOVA vaccination has the potential to generate enduring antigen-specific immune memory (Fig. 9g and S22). Taken together, these results underscore the ability of the DP50-PE6/mOVA vaccine to not only effectively inhibit tumor growth but also activate a robust immune response.

Conclusions

We developed a series of POx-based mRNA delivery vectors (DPm-PEn) *via* a straightforward ring-opening reaction between amino and epoxide molecules. The effects of alkyl chain length and DP on transfection efficiency and cytotoxicity were systematically evaluated. By precisely tuning the polymer-to-mRNA mass ratio, we identified two optimal candidates—DP25-PE6 and DP50-PE6—for subsequent studies. DP25-PE6 and DP50-PE6 facilitated robust mRNA delivery and high gene expression (1.0×10^8–1.0×10^{10} RLU per mg) in various cell lines *in vitro*. Upon intramuscular injection, both DP25-PE6 and DP50-PE6 successfully mediated mRNA transfection at the injection site, with DP50-PE6 achieving a 3.0-fold higher protein expression compared to DP25-PE6. Following intravenous administration, DP50-PE6 selectively transfected the spleen and induced 2.6-fold higher protein expression than DP25-PE6. In the B16-OVA melanoma model, both intramuscular and intravenous administration of DP50-PE6/mOVA vaccines in combination with anti-PD-1 suppressed tumor growth, achieving tumor suppression rate (TSR%) of 81% and 90%, respectively. Immunological analysis revealed that DP50-PE6/mRNA vaccine in combination with anti-PD-1 induced a strong immune response by promoting the maturation of DCs in lymph nodes, enhancing T cell responses, increasing tumor-infiltrating T cells, and establishing durable immune memory responses. This study highlights the significant potential of POx-based vectors in mRNA delivery, with DP50-PE6 demonstrating especially promising performance.

Ethical statement

All animal experiments adhered to the guidelines sanctioned by the Animal Welfare and Ethics Committee of Changchun Institute of Applied Chemistry, Chinese Academy of Sciences (20230078).

Author contributions

Kuncheng Lv: conceptualization, methodology, original draft preparation. Yibo Qi: methodology. Hanqin Zhao and Yuyan Zhang: visualization, investigation. Ziyue An and Sheng Ma: formal analysis. Wantong Song: project administration, writing, funding acquisition, validation.

Conflicts of interest

The authors declare that they have no conflicts of interest in this work.

Data availability

The data supporting this article have been included as part of the supplementary information (SI). Supplementary information is available. See DOI: https://doi.org/10.1039/d5sc04801j.

Acknowledgements

This work was supported by National Key Research and Development Program of China (2024YFB3814800, 2024YFA1212200), National Natural Science Foundation of China (Grant No. 22222509, 22375198, W2412020), and Jilin Provincial International Cooperation Key Laboratory of Biomedical Polymers (YDZJ202402077CXJD).

Notes and references

1 E. J. Sayour, D. Boczkowski, D. A. Mitchell and S. K. Nair, Cancer mRNA vaccines: clinical advances and future opportunities, *Nat. Rev. Clin. Oncol.*, 2024, **21**, 489–500.
2 H. Parhiz, E. N. Atochina-Vasserman and D. Weissman, mRNA-based therapeutics: looking beyond COVID-19 vaccines, *Lancet*, 2024, **403**, 1192–1204.
3 R. S. Riley, M. V. Kashyap, M. M. Billingsley, B. White, M.-G. Alameh, S. K. Bose, P. W. Zoltick, H. Li, R. Zhang, A. Y. Cheng, D. Weissman, W. H. Peranteau and M. J. Mitchell, Ionizable lipid nanoparticles for in utero mRNA delivery, *Sci. Adv.*, 2021, **7**, eaba1028.
4 M. S. Gebre, L. A. Brito, L. H. Tostanoski, D. K. Edwards, A. Carfi and D. H. Barouch, Novel approaches for vaccine development, *Cell*, 2021, **184**, 1589–1603.
5 M. J. Mulligan, K. E. Lyke, N. Kitchin, J. Absalon, A. Gurtman, S. Lockhart, K. Neuzil, V. Raabe, R. Bailey, K. A. Swanson, P. Li, K. Koury, W. Kalina, D. Cooper, C. Fontes-Garfias, P.-Y. Shi, Ö. Türeci, K. R. Tompkins, E. E. Walsh, R. Frenck, A. R. Falsey, P. R. Dormitzer, W. C. Gruber, U. Şahin and K. U. Jansen, Phase I/II study of COVID-19 RNA vaccine BNT162b1 in adults, *Nature*, 2020, **586**, 589–593.
6 K. S. Corbett, D. K. Edwards, S. R. Leist, O. M. Abiona, S. Boyoglu-Barnum, R. A. Gillespie, S. Himansu, A. Schäfer, C. T. Ziwawo, A. T. DiPiazza, K. H. Dinnon, S. M. Elbashir, C. A. Shaw, A. Woods, E. J. Fritch, D. R. Martinez, K. W. Bock, M. Minai, B. M. Nagata, G. B. Hutchinson, K. Wu, C. Henry, K. Bahl, D. Garcia-Dominguez, L. Ma, I. Renzi, W.-P. Kong, S. D. Schmidt, L. Wang, Y. Zhang, E. Phung, L. A. Chang, R. J. Loomis, N. E. Altaras, E. Narayanan, M. Metkar, V. Presnyak, C. Liu, M. K. Louder, W. Shi, K. Leung, E. S. Yang, A. West, K. L. Gully, L. J. Stevens, N. Wang, D. Wrapp, N. A. Doria-Rose, G. Stewart-Jones, H. Bennett, G. S. Alvarado, M. C. Nason, T. J. Ruckwardt, J. S. McLellan, M. R. Denison, J. D. Chappell, I. N. Moore, K. M. Morabito, J. R. Mascola, R. S. Baric, A. Carfi and B. S. Graham, SARS-CoV-2 mRNA vaccine design enabled by prototype pathogen preparedness, *Nature*, 2020, **586**, 567–571.
7 K. A. Hajj and K. A. Whitehead, Tools for translation: non-viral materials for therapeutic mRNA delivery, *Nat. Rev. Mater.*, 2017, **2**, 17056.
8 N. Pardi, M. J. Hogan, F. W. Porter and D. Weissman, mRNA vaccines — a new era in vaccinology, *Nat. Rev. Drug Discovery*, 2018, **17**, 261–279.
9 X. Hou, T. Zaks, R. Langer and Y. Dong, Lipid nanoparticles for mRNA delivery, *Nat. Rev. Mater.*, 2021, **6**, 1078–1094.
10 J. Houseley and D. Tollervey, The Many Pathways of RNA Degradation, *Cell*, 2009, **136**, 763–776.
11 T. Harayama and H. Riezman, Understanding the diversity of membrane lipid composition, *Nat. Rev. Mol. Cell Biol.*, 2018, **19**, 281–296.
12 Z. Li, L. Amaya, R. Pi, S. K. Wang, A. Ranjan, R. M. Waymouth, C. A. Blish, H. Y. Chang and P. A. Wender, Charge-altering releasable transporters enhance mRNA delivery *in vitro* and exhibit *in vivo* tropism, *Nat. Commun.*, 2023, **14**, 6983.
13 A. Gupta, J. L. Andresen, R. S. Manan and R. Langer, Nucleic acid delivery for therapeutic applications, *Adv. Drug Delivery Rev.*, 2021, **178**, 113834.
14 P. Huang, H. Deng, C. Wang, Y. Zhou and X. Chen, Cellular Trafficking of Nanotechnology-Mediated mRNA Delivery, *Adv. Mater.*, 2024, **36**, 2307822.
15 Y. Ma and O. S. Fenton, An Efficacy and Mechanism Driven Study on the Impact of Hypoxia on Lipid Nanoparticle Mediated mRNA Delivery, *J. Am. Chem. Soc.*, 2023, **145**, 11375–11386.
16 R. A. Meyer, S. Y. Neshat, J. J. Green, J. L. Santos and A. D. Tuesca, Targeting strategies for mRNA delivery, *Mater. Today Adv.*, 2022, **14**, 100240.
17 P. Huang, H. Deng, Y. Zhou and X. Chen, The roles of polymers in mRNA delivery, *Matter*, 2022, **5**, 1670–1699.
18 J. Zuo, Z. Lu, J. Guo, R. Zhao, T. Zhang, Z. Wang, Y. Yuan, J. Deng, J. Yuan and X. Zhang, Bioinspired and bioengineered nucleic acid drug carriers, *Sci. China Mater.*, 2024, **67**, 2393–2413.
19 Y. Jia, X. Wang, L. Li, F. Li, J. Zhang and X.-J. Liang, Lipid Nanoparticles Optimized for Targeting and Release of Nucleic Acid, *Adv. Mater.*, 2024, **36**, 2305300.
20 L. R. Baden, H. M. E. Sahly, B. Essink, K. Kotloff, S. Frey, R. Novak, D. Diemert, S. A. Spector, N. Rouphael, C. B. Creech, J. McGettigan, S. Khetan, N. Segall, J. Solis, A. Brosz, C. Fierro, H. Schwartz, K. Neuzil, L. Corey, P. Gilbert, H. Janes, D. Follmann, M. Marovich, J. Mascola, L. Polakowski, J. Ledgerwood, B. S. Graham, H. Bennett, R. Pajon, C. Knightly, B. Leav, W. Deng, H. Zhou, S. Han, M. Ivarsson, J. Miller and T. Zaks, Efficacy and Safety of the mRNA-1273 SARS-CoV-2 Vaccine, *N. Engl. J. Med.*, 2021, **384**, 403–416.
21 F. P. Polack, S. J. Thomas, N. Kitchin, J. Absalon, A. Gurtman, S. Lockhart, J. L. Perez, G. P. Marc, E. D. Moreira, C. Zerbini, R. Bailey, K. A. Swanson, S. Roychoudhury, K. Koury, P. Li,

W. V. Kalina, D. Cooper, R. W. Frenck, L. L. Hammitt, Ö. Türeci, H. Nell, A. Schaefer, S. Ünal, D. B. Tresnan, S. Mather, P. R. Dormitzer, U. Şahin, K. U. Jansen and W. C. Gruber, Safety and Efficacy of the BNT162b2 mRNA Covid-19 Vaccine, *N. Engl. J. Med.*, 2020, **383**, 2603–2615.

22 M. Qiu, Y. Tang, J. Chen, R. Muriph, Z. Ye, C. Huang, J. Evans, E. P. Henske and Q. Xu, *Lung-selective mRNA delivery of synthetic lipid nanoparticles for the treatment of pulmonary lymphangioleiomyomatosis*, Proceedings of the National Academy of Sciences, 2022, vol. 119, p. e2116271119.

23 N. Chaudhary, D. Weissman and K. A. Whitehead, mRNA vaccines for infectious diseases: principles, delivery and clinical translation, *Nat. Rev. Drug Discovery*, 2021, **20**, 817–838.

24 M. Qiu, Z. Glass, J. Chen, M. Haas, X. Jin, X. Zhao, X. Rui, Z. Ye, Y. Li, F. Zhang and Q. Xu, *Lipid nanoparticle-mediated codelivery of Cas9 mRNA and single-guide RNA achieves liver-specific in vivo genome editing of Angptl3*, Proceedings of the National Academy of Sciences, 2021, vol. 118, p. e2020401118.

25 P. Zhao, X. Hou, J. Yan, S. Du, Y. Xue, W. Li, G. Xiang and Y. Dong, Long-term storage of lipid-like nanoparticles for mRNA delivery, *Bioact. Mater.*, 2020, **5**, 358–363.

26 J. Kim, Y. Eygeris, M. Gupta and G. Sahay, Self-assembled mRNA vaccines, *Adv. Drug Delivery Rev.*, 2021, **170**, 83–112.

27 H. Zhao, S. Ma, Y. Qi, Y. Gao, Y. Zhang, M. Li, J. Chen, W. Song and X. Chen, A polyamino acid-based phosphatidyl polymer library for *in vivo* mRNA delivery with spleen targeting ability, *Mater. Horiz.*, 2024, **11**, 2739–2748.

28 P. B. Tiwade, Y. Ma, R. VanKeulen-Miller and O. S. Fenton, A Lung-Expressing mRNA Delivery Platform with Tunable Activity in Hypoxic Environments, *J. Am. Chem. Soc.*, 2024, **146**, 17365–17376.

29 E. W. Kavanagh, S. Y. Tzeng, N. Sharma, G. R. Cutting and J. J. Green, Ligand-free biodegradable poly(beta-amino ester) nanoparticles for targeted systemic delivery of mRNA to the lungs, *Biomaterials*, 2025, **313**, 122753.

30 J. C. Kaczmarek, A. K. Patel, K. J. Kauffman, O. S. Fenton, M. J. Webber, M. W. Heartlein, F. DeRosa and D. G. Anderson, Polymer-Lipid Nanoparticles for Systemic Delivery of mRNA to the Lungs, *Angew. Chem., Int. Ed.*, 2016, **55**, 13808–13812.

31 W. Yang, L. Mixich, E. Boonstra and H. Cabral, Polymer-Based mRNA Delivery Strategies for Advanced Therapies, *Adv. Healthcare Mater.*, 2023, **12**, 2202688.

32 Y. Xu, J. Chen, J. Ding, J. Sun, W. Song, Z. Tang, C. Xiao and X. Chen, Synthetic Polymers for Drug, Gene, and Vaccine Delivery, *Polym. Sci. Technol.*, 2025, **1**, 171–220.

33 Z. Luo, X. Zhao, M. Zhou, J. Zou, X. Xiao, L. Liu, J. Xie, Y. Wu, W. Zhang and R. Liu, Peptide-mimicking poly(2-oxazoline)s as adjuvants to enhance activities and antibacterial spectrum of polymyxin B, *Sci. China Mater.*, 2024, **67**, 991–999.

34 L. Yang, F. Wang, P. Ren, T. Zhang and Q. Zhang, Poly(2-oxazoline)s: synthesis and biomedical applications, *Macromol. Res.*, 2023, **31**, 413–426.

35 R. Hoogenboom, The future of poly(2-oxazoline)s, *Eur. Polym. J.*, 2022, **179**, 111521.

36 K. Lv, S. Ma, L. Liu, H. Chen, Z. Huang, Z. Zhu, Y. Qi and W. Song, Peptide nanovaccine conjugated *via* a retro-Diels–Alder reaction linker for overcoming the obstacle in lymph node penetration and eliciting robust cellular immunity, *J. Mater. Chem. B*, 2024, **12**, 5848–5860.

37 J. F. R. Van Guyse, S. Abbasi, K. Toh, Z. Nagorna, J. Li, A. Dirisala, S. Quader, S. Uchida and K. Kataoka, Facile generation of heterotelechelic poly(2-oxazoline)s towards accelerated exploration of poly(2-oxazoline)-based nanomedicine, *Angew. Chem., Int. Ed.*, 2024, **63**, e202404972.

38 A. J. D. S. Sanchez, D. Loughrey, E. S. Echeverri, S. G. Huayamares, A. Radmand, K. Paunovska, M. Hatit, K. E. Tiegreen, P. J. Santangelo and J. E. Dahlman, Substituting Poly(ethylene glycol) Lipids with Poly(2-ethyl-2-oxazoline) Lipids Improves Lipid Nanoparticle Repeat Dosing, *Adv. Healthcare Mater.*, 2024, **13**, 2304033.

39 C. T. Holick, T. Klein, C. Mehnert, F. Adermann, I. Anufriev, M. Streiber, L. Harder, A. Traeger, S. Hoeppener, C. Franke, I. Nischang, S. Schubert and U. S. Schubert, Poly(2-ethyl-2-oxazoline) (POx) as Poly(ethylene glycol) (PEG)-Lipid Substitute for Lipid Nanoparticle Formulations, *Small*, 2025, **21**, 2411354.

40 X. He, T. J. Payne, A. Takanashi, Y. Fang, S. D. Kerai, J. P. Morrow, H. Al-Wassiti, C. W. Pouton and K. Kempe, Tailored Monoacyl Poly(2-oxazoline)- and Poly(2-oxazine)-Lipids as PEG-Lipid Alternatives for Stabilization and Delivery of mRNA-Lipid Nanoparticles, *Biomacromolecules*, 2024, **25**, 4591–4603.

41 Q. Shuai, F. Zhu, M. Zhao and Y. Yan, mRNA delivery *via* non-viral carriers for biomedical applications, *Int. J. Pharm.*, 2021, **607**, 121020.

42 J. Rejman, G. Tavernier, N. Bavarsad, J. Demeester and S. C. De Smedt, mRNA transfection of cervical carcinoma and mesenchymal stem cells mediated by cationic carriers, *J. Controlled Release*, 2010, **147**, 385–391.

43 H. Zhang, S. C. De Smedt and K. Remaut, Fluorescence Correlation Spectroscopy to find the critical balance between extracellular association and intracellular dissociation of mRNA complexes, *Acta Biomater.*, 2018, **75**, 358–370.

44 J. Casper, S. H. Schenk, E. Parhizkar, P. Detampel, A. Dehshahri and J. Huwyler, Polyethylenimine (PEI) in gene therapy: Current status and clinical applications, *J. Controlled Release*, 2023, **362**, 667–691.

45 D. Fischer, Y. X. Li, B. Ahlemeyer, J. Krieglstein and T. Kissel, In vitro cytotoxicity testing of polycations: influence of polymer structure on cell viability and hemolysis, *Biomaterials*, 2003, **24**, 1121–1131.

46 H. Lv, S. Zhang, B. Wang, S. Cui and J. Yan, Toxicity of cationic lipids and cationic polymers in gene delivery, *J. Controlled Release*, 2006, **114**, 100–109.

47 Y. Jin, X. Wang, A. P. E. Kromer, J. T. Müller, C. Zimmermann, Z. Xu, A. Hartschuh, F. Adams and O. M. Merkel, Role of Hydrophobic Modification in Spermine-Based Poly(β-amino ester)s for siRNA Delivery and Their Spray-Dried Powders for Inhalation and Improved Storage, *Biomacromolecules*, 2024, **25**, 4177–4191.
48 S. Cesana, J. Auernheimer, R. Jordan, H. Kessler and O. Nuyken, First Poly(2-oxazoline)s with Pendant Amino Groups, *Macromol. Chem. Phys.*, 2006, **207**, 183–192.
49 M. Zhou, Z. Ji, X. Xiao, L. Liu, R. Cui, Z. Luo, Z. Cong and R. Liu, Controllable and facile synthesis of poly(2-oxazoline)s using trimethylsilyl trifluoromethanesulfonate as the initiator, *Polym. Chem.*, 2023, **14**, 1064–1071.
50 G. Moura-Letts and J. Lizza, Solvent-Directed Epoxide Opening with Primary Amines for the Synthesis of β-Amino Alcohols, *Synthesis*, 2016, **49**, 1231–1242.
51 D. J. Chen, B. S. Majors, A. Zelikin and D. Putnam, Structure–function relationships of gene delivery vectors in a limited polycation library, *J. Controlled Release*, 2005, **103**, 273–283.
52 Y. Li, Z. He, X. Wang, Z. Li, M. Johnson, R. Foley, A. Sigen, J. Lyu and W. Wang, Branch Unit Distribution Matters for Gene Delivery, *ACS Macro Lett.*, 2023, **12**, 780–786.
53 K. Shin, H.-W. Suh, A. Suberi, C.-H. Whang, M. Ene, J. Grundler, M. K. Grun and W. M. Saltzman, Branching in poly(amine-co-ester) polyplexes impacts mRNA transfection, *Biomaterials*, 2024, **311**, 122692.
54 S. Liu, Q. Cheng, T. Wei, X. Yu, L. T. Johnson, L. Farbiak and D. J. Siegwart, Membrane-destabilizing ionizable phospholipids for organ-selective mRNA delivery and CRISPR–Cas gene editing, *Nat. Mater.*, 2021, **20**, 701–710.
55 H. J. Kim, S. Ogura, T. Otabe, R. Kamegawa, M. Sato, K. Kataoka and K. Miyata, Fine-Tuning of Hydrophobicity in Amphiphilic Polyaspartamide Derivatives for Rapid and Transient Expression of Messenger RNA Directed Toward Genome Engineering in Brain, *ACS Cent. Sci.*, 2019, **5**, 1866–1875.